

Implications of Changing the Cd-Ge-Se Thin Film Thickness Deposited by Thermal Evaporation Technique on Structural and Optical Properties for Optoelectronic Applications

Abdel-naser A. Alfaqeer
Physics Department
Faculty of Science and Education
Saba Region University
Marib, Yemen

A.M. Al-Rebati
Physics Department
Faculty of Science and Education
Saba Region University
Marib, Yemen

M. A. Dabban
Physics Department
Faculty of Science
University of Aden
Aden, Yemen

Abstract:- The present research article examined how the thickness of $\text{Cd}_2\text{Ge}_8\text{Se}_{90}$ thin films affected their structural and optical characteristics. On pre-cleaned glass substrates, the pristine amorphous $\text{Cd}_2\text{Ge}_8\text{Se}_{90}$ thin films of varying thicknesses ($d=374, 516, \text{ and } 816 \text{ nm}$) were synthesized. Swanepoel's strategy was employed to explore the optical characteristics in terms of film thickness, such as the band gap energy (Tauc's energy) and band tail energy (Urbach's energy). Also, optical constants, including the refractive index, n , and extinction coefficient (absorption index, k), depend on transmittance spectroscopy. An indirect optical transition mechanism is observable, according to the assessment of the absorption spectra of the thin films under study. As layer thickness increased, the optical band gap shrank, but the tail energy showed a different pattern of this behavior. The refractive index dispersion was characterized using the Wemple-DiDomenico single oscillator concept, and the dispersion parameters were derived. Oscillator and dispersion energies rise as a film's thickness does. Other dielectric parameters including the high-frequency constant, the ratio of free charge carrier concentration to effective mass, plasma frequency, and single oscillator strength are all significantly influenced by thickness.

Keywords:- Cd-Ge-Se Thin Films; Optical Parameters; Optical Constants; Dispersion Parameters.

I. INTRODUCTION

Chalcogens based mainly on sulfur, tellurium, and selenium have received great attention from researchers interested in physics and chemistry specifically, as these compounds have a major role in various modern applications [1]. It is not surprising because the optical,

electrical, thermal, and magnetic properties of these materials make them applicable in several fields including detectors, solar cells, transistors, sensors, control devices, reflectors, and thermal insulators [2,3]. Also, impurities significantly affect amorphous glass's conduction mechanism and structural form. In chalcogenide glasses, impurities have a significant role in the fabrication of glassy semiconductors and in changing the thermal, mechanical, electrical, and optical properties, which contributes to the development of new premium materials. Chalcogenide glasses differ from one another in their composition, chemical nature, and concentration of impurities [2, 4].

Various chalcogenide glasses have been studied for their effect on impurities [5-8]. Due to a lack of long-range order and various intrinsic defects, mobility gaps in these glasses are typically characterized by localized states. In many cases, Cd addition changes the structural and physical properties of Se-Ge chalcogenide glasses [9-14]. A wide range of studies had not been conducted on thermally deposited $\text{Cd}_2\text{Ge}_8\text{Se}_{90}$ films. Film thickness plays an important role in enhancing the structural and optical properties of $\text{Cd}_2\text{Ge}_8\text{Se}_{90}$ films. For determining the thickness and refractive index of transparent regions, the Swanepoel method is widely used. A strong absorbing region's transmission and reflection spectra are used to determine the extinction coefficient (k). Indirect transitions are applicable to $\text{Cd}_2\text{Ge}_8\text{Se}_{90}$ thin films, according to an assessment of data on light absorption. We explore refractive index dispersion using the Wemple-Didomenico single-oscillator model.

II. EXPERIMENTAL DETAILS

The bulk glassy material was produced by alloying extremely pure Cd, Se, and Ge elements 99.999% (Sigma Company, Cairo, Egypt) to make $Cd_2Ge_8Se_{90}$ using the well-known melt quenching process. These components were weighed in accordance with their atomic percentages using an electrically sensitive scale with a 0.1 mg accuracy. In order to achieve a high degree of homogeneity for the finished product, the weighted elements were placed into a clean, evacuated (10^{-6} mbar), silica tube and heated at 980 °C for 20 hours in a furnace that vibrates frequently throughout the synthesis process. After synthesis, glassy compositions were created by cooling the molten material in an ice-cold water bath. The thermal evaporation technique was employed to generate thin coatings on clean glass substrates positioned in an easily rotatable holder. All films were deposited at room temperature. Due to the rotation speed, a uniform distribution of film thickness of around 374, 516, and 816 nm was created. During film deposition, the Edward Coating Unit (306A) vacuum chamber was pumped down to (10^{-5} Torr). In order to prevent the samples from oxidizing during annealing, the films were annealed in a Pyrex tube furnace for 30 minutes at 473 -573K under a flow of pure nitrogen. During deposition, the thickness of film samples was monitored using a thickness monitor (FTM2).

The chemical components of the formed films was assessed using an energy dispersive X-ray analysis (EDX) instrument attached to a scanning electron microscope (SEM), Jeol (JSM)-5400type. The structure of the film was confirmed using a Philips X-ray diffractometer (PW1710, with Cu as the target and Ni as a filter, $\lambda = 1.5418$ at 40 kV and 30 mA). With a scan rate of $0.06^\circ/\text{min}$, scattering angles (2θ) between 4° and 90° at room temperature were observed. The films' transmittance $T(\lambda)$ and reflectance $R(\lambda)$ were measured optically at normal incidence in the wavelength range of 350–2500 nm using a double-beam spectrophotometer (JASCO Corp., V-570, Rev.1.00.) which is attached to a PC data acquisition system and coupled with a specular reflection stage. The obtained results of $R(\lambda)$ and $T(\lambda)$ are then used to investigate the optical properties.

III. RESULTS AND DISCUSSION

A. Structural Identification of Samples

EDX was used for the empirical analysis of $Cd_2Ge_8Se_{90}$ films. Cd, Ge, and Se were discovered through elemental analysis. As shown in **Fig. 1**, the ratios of the constituent elements in the examined thin films were comparable to the target compositions and contained no unexpected elements. The table incorporated into **Fig. 1** displays the evaluation percent of elements in comparison to theoretical ones. Additionally, **Fig. 2** shows the X-ray diffraction patterns for the compositions under investigation as thin films and powders. The amorphous (glassy) character of all samples was confirmed by the absence of discernible structural peaks in these patterns.

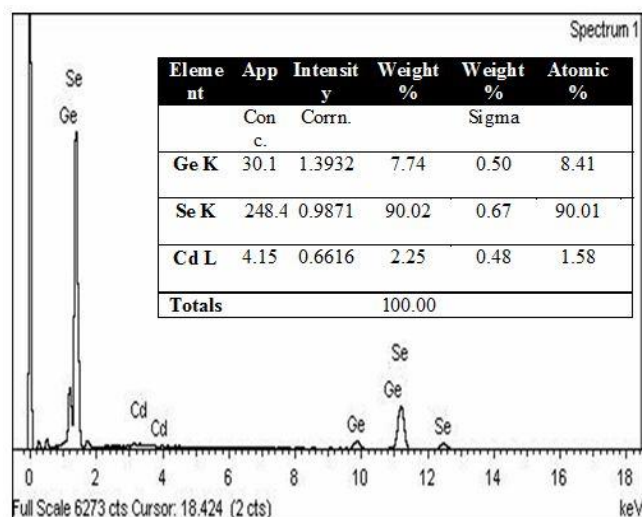


Fig 1 Energy Dispersive X-ray (EDX)- of $Cd_2Ge_8Se_{90}$ Composition

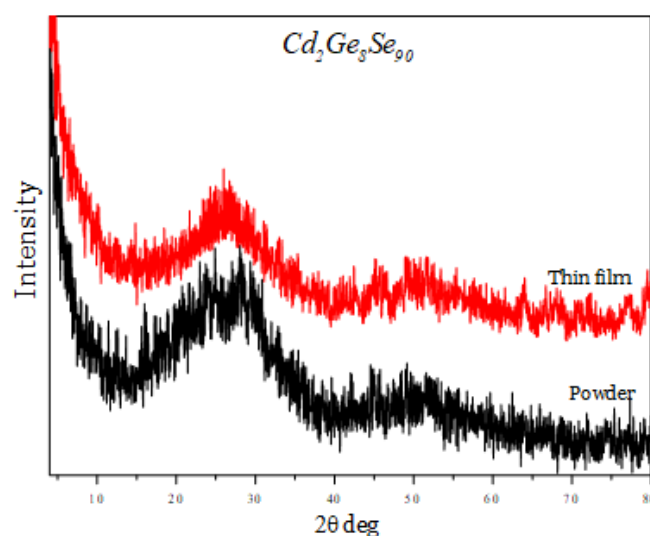


Fig 2 X-ray Diffraction Patterns of $Cd_2Ge_8Se_{90}$ Powder and thin Film form.

B. Optical Analysis of $Cd_2Ge_8Se_{90}$ thin Films.

It is important to pay close attention to the optical absorption of the compositions being studied, notably the absorption edge, while analyzing the electrical structure of chalcogenide glass. The spectral distribution of the refractive index and extinction coefficient was computed using Swanepoel's method [15]. While the optical dispersion parameters dispersion energy, E_d , and oscillator energy, E_o were estimated by studying the refractive index, n data below the inter-band absorption edge, the optical energy gap, E_g , was computed by evaluating the absorption coefficient spectroscopy.

➤ The Optical Spectra

The transmittance of the studied films at various thicknesses was tested using un-polarized light at normal incidence in the wavelength range (350–2500 nm). **Fig. 3a** presents the findings. As the film thickness rises, the interference fringes are increasingly noticeable. As an illustration, **Fig. 3b** portrays the transmittance and

reflectance spectra distribution pathways at a thickness of 816 nm. As seen in the image, films become transparent at longer wavelength areas, when $k=0$, $T+R=1$, and no light is absorbed. The top and lower envelopes were created using OriginLab envelopes Origin version 2019 to research the optical constants, as seen in **Fig. 3b**.

➤ *The Dispersion Curves of Refractive Index (n) And thickness (d) Determination:*

The refractive index, n , and film thickness, d , are all determined based on the upper and lower envelopes of their transmittance spectrum with interference fringes [15] and the well-known Swanepoel method. The spectral distribution of n for all thicknesses examined is portrayed in **Fig. 4**.

➤ *The Spectral Distribution of the Absorption Coefficient (α) and Extinction Index, k :*

Investigating the spectral distribution of a semiconductor's absorption coefficient close to its primary edge is essential for figuring out the kinds of transitions the semiconductor is permitted to make as well as its energy bands. According to the refractive index and thickness of the film over the range (400-2500)nm, it is possible to compute the absorbance ($x=\exp(-ad)$) via the transmission spectrum $T_\alpha = \sqrt{T_M T_m}$, [as incarnated in **Fig.3b**], using Connell and Lewis' equation [16]:

$$\left[\alpha = -\frac{1}{d} \ln \left[\frac{p + [P^2 + 2QT_\alpha(1 - R_2R_3)]^{1/2}}{Q} \right] \right] \quad (1)$$

where $p = (R_1 - 1)(R_2 - 1)(R_3 - 1)$
 and $Q = 2T_\alpha(R_1R_2 + R_1R_3 - 2R_1R_2R_3)$
 $R_1 = \left[\frac{1-n}{1+n} \right]^2, R_2 = \left[\frac{n-s}{n+s} \right]^2, R_3 = \left[\frac{1-s}{1+s} \right]^2$

In these equations: R_1 represents the reflectance of the air-film, R_2 incarnates the reflectance of the film-substrate interface, and R_3 is the reflectance of the substrate-air interface. Also, the extinction coefficient, k which represent of the imaginary part of optical constants, is extracted via the formula ($\alpha = 4\pi k / \lambda$). **Fig. 5 and 6**, illustrate the spectral distributions of α and k for studied films at different thicknesses.

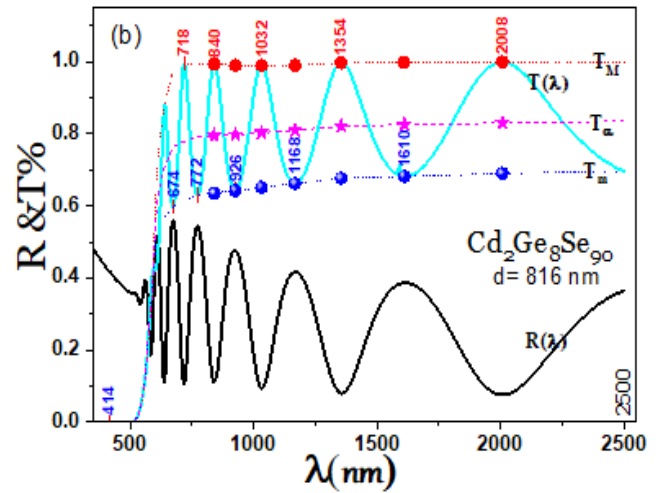
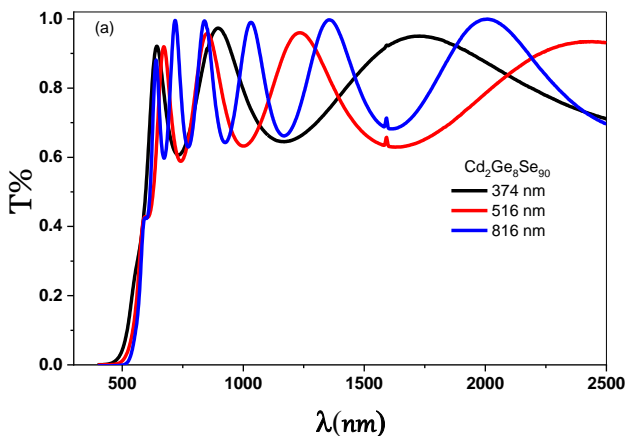


Fig 3 Spectral Distribution for (a) Transmittance $T(\lambda)$ for all $Cd_2Ge_8Se_{90}$ Films and (b) Transmittance $T(\lambda)$ and Reflectance $R(\lambda)$ for Thickness 816 nm.

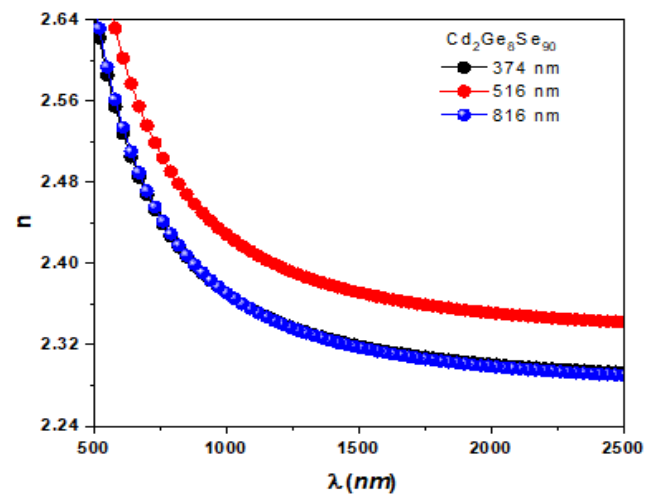


Fig 4 Spectral Dependence of the Refractive Index, n for $Cd_2Ge_8Se_{90}$ Thin Films.

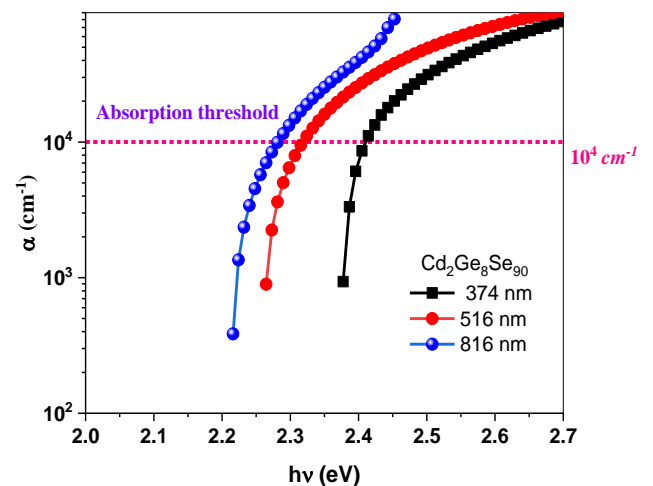


Fig 5 Spectral Dependence of the Absorption α for $Cd_2Ge_8Se_{90}$ Thin Films

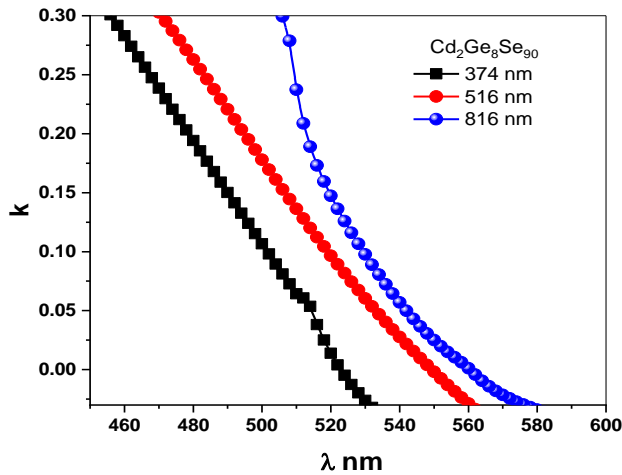


Fig 6 Spectral Dependence of the Absorption Index k for $Cd_2Ge_8Se_{90}$ Thin Films

➤ *Optical Absorption Edge and Optical Energy Gap:*

The absorption coefficient (α) plot as a function of photon energy ($h\nu$) of the incident photons for the analyzed thin films is illustrated in Fig. 5 where each curve of this figure is divided into two regions [17].

$$\alpha h\nu = A (h\nu - E_g^{opt})^r \quad (2)$$

The main absorption coefficient pathway is at the higher values in this diagram, namely, for $(\alpha(\nu) \geq 10^4 \text{ cm}^{-1})$. According to Tauc's power law behavior, this leads to optical transitions between extended states in both the valence and conduction sectors [18]. In above formula, A is the film quality, E_g^{opt} represents the material's optical energy gap, and r incarnates a characterized value of optical transition type. For the allowed direct transition in this analysis, r is $1/2$, while for the allowed indirect transition has the value which equals to 2 . The value of E_g^{opt} is extracted from a diagram of $(\alpha h\nu)^{1/2}$ vs. $h\nu$ plotted in Fig. 7 for the allowed indirect transitions. The edge width parameter value A is computed from the slopes of these linear parts. The extracted values of E_g^{opt} and A are listed and reported in Table 1. For the lower values of the absorption coefficient, namely, that in it $\alpha(\nu) < 10^4 \text{ cm}^{-1}$, Urbach's rule usually applies to absorption at lower photon energies according to the following equation [19]:

$$\alpha(\nu) = \alpha_o \exp(h\nu / E_e) \quad (3)$$

The absorption pathways at this point are caused by the main transitions between localized states in any band's exponential tail and extended states in another band in this case [20], where (α_o) represents a constant and (E_e) incarnates the Urbach energy, namely, the width of the tails of localized states in the band gap. This energy generally is the degree of disorder in an amorphous matrix [21].

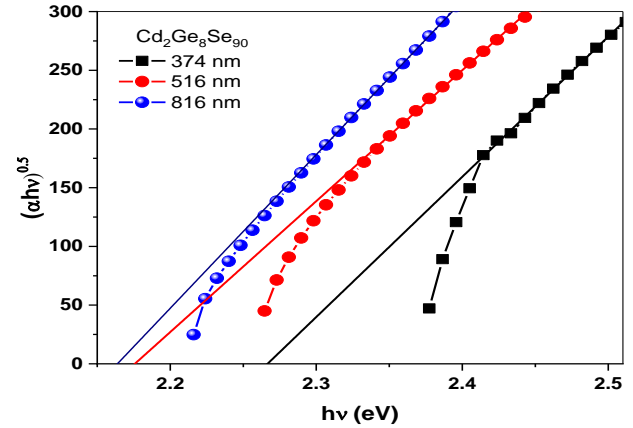


Fig 7 Dependence of $(\alpha h\nu)^{1/2}$ on the Photon Energy $h\nu$ for $Cd_2Ge_8Se_{90}$ Films

From plotting $\ln \alpha$ as a function of $h\nu$, shown in Fig. 8, values of E_e as a function of thickness can be calculated and given in Table 1

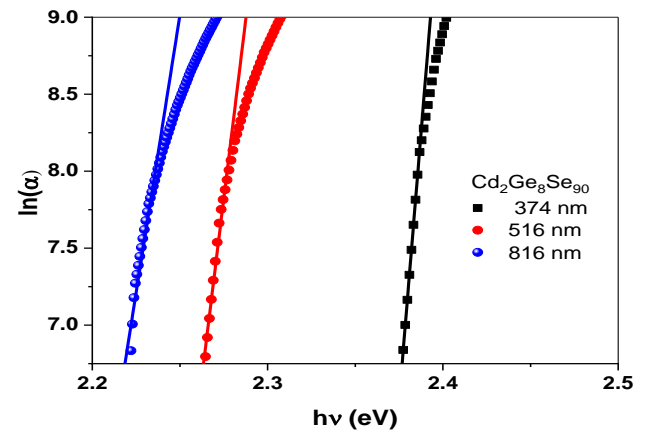


Fig 8 Plots of $\ln \alpha$ as a Function of Photon Energy $h\nu$ for $Cd_2Ge_8Se_{90}$ Films.

According to Table 1, while the tail band energy grows with increasing film thickness, the bandgap energy decreases. The observed energy gap reduction can be explained by the density of states concept in amorphous solids put out by Mott and Davis [22]. The width of localized states near the mobility edge is determined by the degree of disorder and defect present in the amorphous structure. Unsaturated bonds are recognized to be the cause of a variety of faults in amorphous materials. This may lead to increase in the width of the localized states, indicating a decrease in the optical energy gap of the investigated films.

➤ *Dispersion Parameters:*

Dispersion plays a crucial part in the study of optoelectronics since it is a vital factor in the design of fiber optics and spectrally scattering devices. The strong evidence that both crystal structure and ionicity influence the refractive index behaviour of solids in easily understood ways is one aspect that all of these laws have in general, despite the fact that the specifics of them differ greatly [23]. The dispersion parameters were computed by Wemple and Didomenico using a single-oscillator model of the

frequency-dependent dielectric constant. This model can be used to match the following association between a single oscillator's strength and refractive index underneath the bandgap [24, 25]:

$$n^2 = 1 + \frac{E_o E_d}{E_o^2 - (h\nu)^2} \quad (4)$$

Here, E_d and E_o are single oscillator constants, E_o the energy of the effective dispersion oscillator, E_d represents dispersion energy. The last energy measures the average strength of inter band optical transitions.

Table 1 The Parameters E_D , E_o , E_e AND E_g^{opt} For $Cd_2Ge_8Se_9$ Thin Films.

Thickness	E_g^{opt} (eV)	A $cm^{-1} \cdot eV^{-1}$	E_e (eV)	E_o eV	E_o / E_g^{opt}	E_d eV
374 nm	2.26	2707	0.0072	4.08	1.81	17
516 nm	2.18	2426	0.0110	3.96	1.82	17.5
816 nm	2.16	2831	0.0140	4.01	1.86	16.8

Fig. 9 incarnates the plotting of $(n^2 - 1)^{-1}$ against $(h\nu)^2$ for the studied layers. In this diagram, from the yielded straight lines the slope $(E_o E_d)^{-1}$ and the intercept E_o / E_d help in extracting the dispersion parameters. At higher wavelengths, the obtained curves showed a positive divergence from linearity, which is often caused by the negative impact of lattice vibrations on the refractive index [25]. The computed values of E_o and E_d are listed in **Table 1**.

The obtained values of E_d and E_o for the studied compositions have slight differences with those obtained in the related work [26]. This, in turn, can be caused by the different structural characteristics and impurities present in the compositions under investigation.

It is evident from **Table 1** that the average ratio of $E_o / E_g \approx 2$, which is in good agreement with that mentioned by Tanaka formula [27].

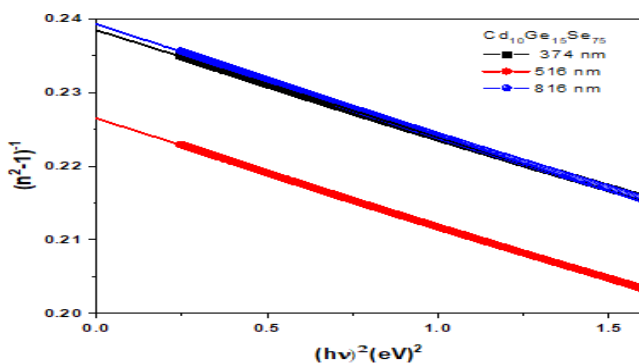


Fig 9 A plot of $(n^2 - 1)^{-1}$ Against $(h\nu)^2$ for $Cd_2Ge_8Se_9$ Films

➤ *Dielectric constant*

The high frequency dielectric constant (ϵ_∞) in this work can be calculated and extracted utilizing the refractive index (n) data analysis employing two fundamental techniques [28]. The first procedure, which is of utmost relevance, depicts the contribution of free carriers as well as the lattice vibrational modes of the dispersion. The second method, on the other hand, is based on the dispersion that results from bound carriers in an empty lattice. With both approaches, a reliable value for the high-frequency dielectric constant was obtained.

• *The First Procedure:*

The following formula is utilized to extract the high frequency constant of dielectric parameters [28,29]

$$n^2 = \epsilon_r = \epsilon_L - \beta \lambda^2 \quad (5)$$

Here, ϵ_r represents the real part of dielectric constant, ϵ_L offers the meaning of the lattice dielectric constant, λ is the wavelength in the range of (400-2500) nm and β extracts from $(e^2 N / 4 \pi^2 \epsilon_o m^* c^2)$ formula, where e is the charge of the electron, N displays the free charge-carrier concentration, ϵ_o is the permittivity of free space, m^* the effective mass of the electrons and c the velocity of light in free space.

It is observed that the dependence of $n^2 = \epsilon_r$ (in the transparent region $k=0$) on λ^2 is linear at longer wavelengths, as shown in **Fig. 10**. The value of ϵ_L and values of N/m^* for the investigated layers are computed from the obtained straight lines and are given in **Table 2**.

• *The Second Procedure:*

The high-frequency features of the studied layers could be analyzed as a single oscillator of wavelength λ_o at high frequency via a simple classical dispersion formula [28].

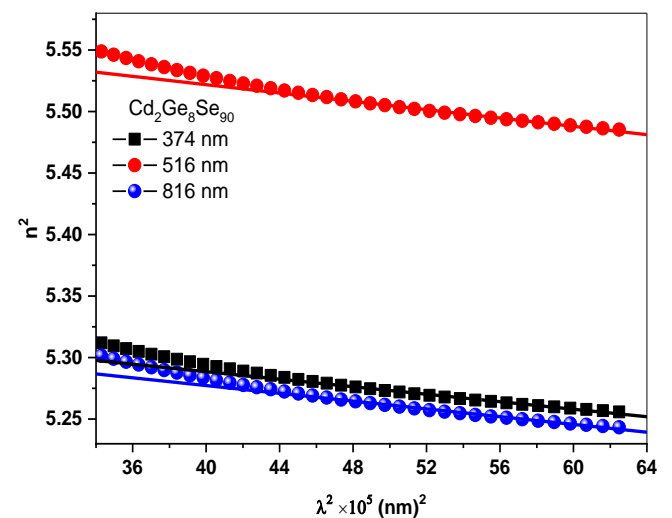


Fig 10 A Plot of ϵ_1 as a Function of λ^2 for $Cd_2Ge_8Se_9$ Films.

Table 2 The parameters $\epsilon_{\infty(L)}$, $\epsilon_{\infty(s)}$, N/m^* , λ_o and ω_p for $Cd_2Ge_8Se_{90}$ films.

Thickness	ϵ_L	N/m^* ($m^{-3}.Kg^{-1}$) $\times 10^{58}$	ω_p (s^{-1}) $\times 10^{14}$	$\lambda_o nm$	$\epsilon_{\infty s}$ $= n_s^2$
374 nm	5.35	1.17	2.51462	311	5.19
516 nm	5.59	1.3	2.59279	321	5.41
816 nm	5.34	1.2	2.56147	317	5.18

If n_s value is the refractive index of an empty lattice at infinite wavelength λ_o , it will vary as:

$$(n_s^2 - 1) / (n^2 - 1) = 1 - (\lambda_o / \lambda)^2 \quad (6)$$

Where λ_o and n_s have been evaluated from plots of $(n^2 - 1)^{-1}$ against λ^{-2} and plotted in **Fig. 11**. The values of n_s^2 can be computed by the noticed lines to the y-axis, while λ_o was extracted from the slopes of the lines of **Fig.11** and **Eq. 6**. **Table 2**. Illustrates the values of $n_s^2 = \epsilon_{\infty(s)}$ and λ_o . The values of ϵ_L and $\epsilon_{\infty(s)}$ extracted by the mentioned approaches are consistent. Despite the differences in procedures, the reason for this agreement is that the lattice-vibrations and plasma frequencies ω_p are well separated from the absorption band-edge frequency. The optical relative dielectric permittivity $\epsilon_{\infty s} = n_s^2$ values found for the examined films are in the same order as those obtained previously [23,26]. Penn's theory [30], is applicable to chalcogenide materials using the following relation:

$$n^2 = 1 + (h \omega_p / E_g^{opt})^2 \quad (7)$$

Here ω_p represents the plasma frequency (a resonant frequency for free oscillations of the electrons about their equilibrium positions), determined by the ratio [31-35]:

$$\omega_p^2 = e^2 N / \epsilon_0 \epsilon_{\infty L} m^* \quad (8)$$

Using our results of N / m^* , ω_p can be computed from **Eq. 9** and listed also in **Table 2**.

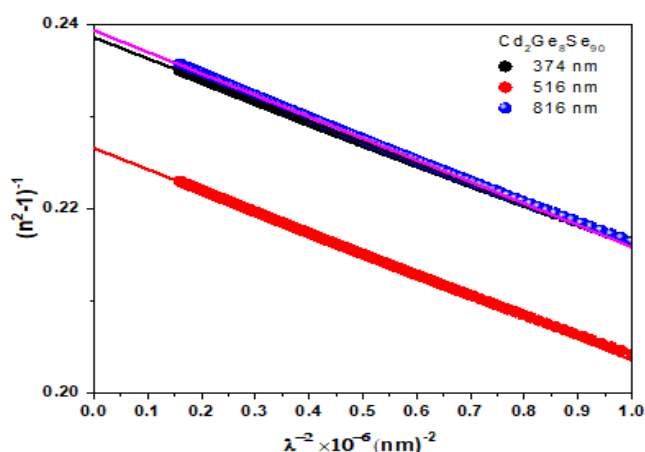


Fig 11 A Plot of $(n^2 - 1)^{-1}$ Against λ^{-2} for $Cd_2Ge_8Se_{90}$ Films

IV. CONCLUSIONS

The glassy alloy $Cd_2Ge_8Se_{90}$ was created using the melt-quench method. The thin films were applied on glass substrates using thermal evaporation. XRD investigations revealed that the powder and as-prepared films are both amorphous. The optical characteristics of $Cd_2Ge_{15}Se_{75}$ were found to be thickness sensitive. As film thickness increases, the optical band gap decreases, while the Urbach energy exhibits the opposite trend. The high-frequency dielectric constant, ϵ_L , and the ratio (N/m^*) exhibited the opposite behavior of the bandgap E_g as the film thickness increased. The optical properties obtained were explained using the Mott-Davis and Wemple-Didomenico models. $Cd_2Ge_8Se_{90}$ thin films are appropriate for a variety of optoelectronic applications based on the optical properties that can be inferred from their measurements.

REFERENCES

- [1]. A. Qasem, Hassan, A. A., Al-nami, S. Y., Alrafai, H. A., & Shaaban, E. R, "Effective role of vacuum annealing in improving structural, optical, and electrical properties of SiO2/Ag/ZnO multilayers deposited by RF sputtering for optoelectronic applications." *Physica Scripta* 98.1 (2022): 015825.
- [2]. Assem, E. E., Ashoura, A., Shaaban, E. R., & Qasem, A. "Implications changing of the CdS window layer thickness on photovoltaic characteristics of n-CdS/i-AgSe/p-CdTe solar cells." *Chalcogenide Letters* 19.11 (2022).
- [3]. F. AL-Maqate, A. Qasem, T. Alomayri, A. Madani, A. Timoumi, D. Hussain, & T. Bruno, "Profundity study on structural and optical properties of heavy oil fly ash (HOFA) doped calcium carbonate (CaCO3) nanostructures and thin films for optoelectronic applications." *Optical Materials* 131 (2022): 112719.
- [4]. Amrani, Mokhtar Ali, Alrafai, H. A., Al-nami, S. Y., Obeidat, F., Alwabhani, F., Alhammadi, M. A., & Qasem, A, "Green synthesis of Size-Controlled copper oxide nanoparticles as catalysts for H2 production from industrial waste aluminum." *International Journal of Energy Research* 46.10 (2022): 14023-14035.
- [5]. Soraya, M. M., Shaaban, E. R., Eman, M., Qasem, A., Mahmoud, S. A., & Yousef, E, "Indium incorporation effects on optical properties of quaternary chalcogenide Se-Zn-Te-In films." *Chalcogenide Letters* 17.3 (2020): 133-145.
- [6]. Mnawer, Ied M., Hemeda, O. M., Hassaan, M. Y., Abdel-Moety, A. S., & Salem, M. M. "Influence of Cr+3 ions substitution on the magnetic and optical properties of NiZnCr Ferrite/PVA/Rhodamine dye nanocomposite film." *Al-Azhar Bulletin of Science* (2022).
- [7]. H. Atyia, N. Hegab, M. Affi, & M. Ismail, "Influence of temperature and frequency on the AC conductivity and dielectric properties for Ge15Se60Bi25 amorphous films." *Journal of alloys and compounds* 574 (2013): 345-353.

- [8]. H. Atyia and N. Hegab. "Optical spectroscopy and dispersion parameters of $\text{Ge}_{15}\text{Se}_{60}\text{X}_{25}$ (X= As or Sn) amorphous thin films." *The European Physical Journal-Applied Physics* 63.1 (2013).
- [9]. M. Alias, M. Faisal, Makadsi, and Z. Al-Ajeli. "The influence of Ge content and annealing temperature on the dc and ac conductivity of $\text{Ge}_x\text{Se}_{1-x}$ thin films." *Turkish Journal of Physics* 27.2 (2003): 133-144.
- [10]. Y.El-Kady,. "The glassy state of the semiconducting system $\text{Ge}_{10}\text{Sb}_x\text{Se}_{90-x}$." *Physica B: Condensed Matter* 275.4 (2000): 344-350.
- [11]. M.Hafiz, A. Othman, M. Elnahass, &A.Al-Motasem, "Composition and electric field effects on the transport properties of Bi doped chalcogenide glasses thin films." *Physica B: Condensed Matter* 390.1-2 (2007): 286-292.
- [12]. H.El-Zahed, and A. El-Korashy. "Influence of composition on the electrical and optical properties of $\text{Ge}_{20}\text{Bi}_x\text{Se}_{80-x}$ films." *Thin Solid Films* 376.1-2 (2000): 236-240.
- [13]. El-Deeb, A. S., A. M. Ismail, and M. Y. Hassaan. "Optical, FTIR, electrical and dielectrical properties of a glass system for smart windows applications." *Optik* 221 (2020): 165358.
- [14]. Ibrahim, Mohamed M., Fanny, M. A., ElBatal, H. A., Hassaan, M. Y., & Abdelghany, A. M, "Spectroscopic studies of preparation conditions role on the shielding properties of MoO_3 -doped $\text{Na}_2\text{O}-\text{ZnO}-\text{P}_2\text{O}_5$." *Journal of the Australian Ceramic Society* (2022): 1-12.
- [15]. A. Qasem, M. Hassaan, M. Moustafa, M. Hammam, H. Zahran, I. Yahia, &E. Shaaban, "Optical and electronic properties for As-60 at.% S uniform thickness of thin films: Influence of Se content." *Optical Materials* 109 (2020): 110257.T
- [16]. A.Y. Abdel-latif, H. Mahfoz Kotb, M. M. Hafiz, M. A. Dabban, "Influence of heat treatment on the structural ,optical and electrical properties of $\text{Cd}_{20}\text{Sn}_{10}\text{Se}_{70}$ thin films", *Materials Science in Semiconductor Processing* 30 (2015) 502–512..
- [17]. B.Alshahrani, S.Nabil, H. Elsaedy, H.Yakout, &A. Qasem, "The Pivotal Role of Thermal Annealing of Cadmium Telluride Thin Film in Optimizing the Performance of CdTe/Si Solar Cells." *Journal of Electronic Materials* 50.8 (2021): 4586-4598.
- [18]. A. Qasem, H. Alrafai, B.Alshahrani, N. Said, A. Hassan, H.Yakout, &E. Shaaban, "Adapting the structural, optical and thermoelectrical properties of thermally annealed silver selenide (AgSe) thin films for improving the photovoltaic characteristics of the fabricated n- $\text{AgSe}/\text{p}-\text{CdTe}$ solar cells." *Journal of Alloys and Compounds* 899 (2022): 163374.
- [19]. H. Elsaedy, A. Hassan, H. Yakout, &A.Qasem, "The significant role of ZnSe layer thickness in optimizing the performance of ZnSe/CdTe solar cell for optoelectronic applications." *Optics & Laser Technology* 141 (2021): 107139.
- [20]. M.Ahmed, A.Bakry, A. Qasem, &H.Dalir, "The main role of thermal annealing in controlling the structural and optical properties of ITO thin film layer." *Optical Materials* 113 (2021): 110866.
- [21]. A. Naim, A.Farha, A.Qasem, &E. Shaaban, "The main role of bismuth in controlling linear and nonlinear optical, electronic and electrical parameters of Se-Ge-Bi thin films." *Journal of Materials Science: Materials in Electronics* 32.6 (2021): 6866-6882.
- [22]. Mnawe, Ied Mohammed, Hassaan, M. Y., Hemed, O. M., & Abdel-Moety, A. S, "XRD, FTIR And Electrical Properties Investigation Of Ni0. 6 Zn0. 4 Crx Fe2-X O4 Thin Films." *Nveo-Natural Volatiles & Essential Oils Journal| NVEO* (2022): 1617-1632.
- [23]. H. Elsaedy, A.Qasem, M.Mahmoud, H. Yakout, &S. Abdelaal, "The precise role of UV exposure time in controlling the orbital transition energies, optical and electrical parameters of thermally vacuum evaporated $\text{Se}_{50}\text{Te}_{50}$ thin film." *Optical Materials* 115 (2021): 111053.
- [24]. S. H. Wemple, M. Didomenico, Behavior of the electronic dielectric constant in covalent and ionic materials, *Phys. Rev. B* 3 (1971) 1338.
- [25]. S. H. Wemple, Refractive-index behavior of amorphous semiconductors and glasses, *Phys. Rev. B* 7 (1973) 3767.
- [26]. Shreif, A., Farag, M. A., El-Sherbiny, M. A., & Hassaan, M. Y, "Effect of Zr ions on the structure and optical properties of lithium borosilicate molybdate glass system." *Ceramics International* (2022).
- [27]. K. Tanaka, Structural phase transitions in chalcogenide glasses, *Phys. Rev. B* 39 (1989) 1270.
- [28]. E. Shaaban, M. Hassaan, M. Moustafa, A. Qasem, & G. Ali, &E. S. Yousef, "Investigation of Structural and Optical Properties of Amorphous-Crystalline Phase Transition of $\text{As}_{40}\text{S}_{45}\text{Se}_{15}$ Thin Films." *ActaPhysicaPolonica, A.* 136.3 (2019).
- [29]. H. Mahfoz Kotb, M.A. Dabban, A.Y. Abdel-latif, M.M. Hafiz, "Annealing temperature dependence of the optical and structural properties of selenium-rich Cd-Se thin films", *Journal of Alloys and Compounds*, 512 (2012), Pages 115-120.
- [30]. Alqahtani, A., Alrafai, H. A., Al-Dossari, M., Shaaban, E. R., & Qasem, A, "A profound analysis of structural, thermal, optical, and electrical properties of $\text{Cd}_{50}\text{Pb}_{30}\text{S}_{20}$ composition for optoelectronic devices: implications of changes in film's thickness." *Optical and Quantum Electronics* 55.1 (2023): 1-36.
- [31]. E. Shaaban, M. Hassaan, M. Moustafa, A.Qasem, &G. Ali, "Optical constants, dispersion parameters and non-linearity of different thickness of $\text{As}_{40}\text{S}_{45}\text{Se}_{15}$ thin films for optoelectronic applications." *Optik* 186 (2019): 275-287.
- [32]. A.Gadalla, F. Anas, A.Qasem, E.Yousef, &E. Shaaban, "Optical constants and dispersion parameters of amorphous $\text{Se}_{65-x}\text{As}_{35}\text{S}_x$ thick films for optoelectronics." *Indian Journal of Physics* 95.9 (2021): 1853-1863.

- [33]. Z. Alrowaili, M.Soraya, T. Alsultani, A.Qasem, E.Shaaban, &M.Ezzeldien, "Sn-induced changes in the structure and optical properties of amorphous As–Se–Sn thin films for optical devices." *Applied Physics A* 127.2 (2021): 1-11.
- [34]. Abdalnasser Alfaqeer, Ahmed Irebati, Mehdi Dabban, "Extraction of Optical Constants and Dispersion Parameters of CdTe/CdSe Bi-Layer Thin Films" *The scientific Journal of university of Saba region*, Vo. 5 No. 1 -December 2022.
- [35]. Saudi, H. A., Hassaan, M. Y., Tarek, E., & Borham, E, "Development of advanced, transparent radiation shielding glass possessing phosphate and lead ions in the glassy matrix." *Journal of Optics* 49.4 (2020): 438-445.